DEVELOPMENT OF THE VALVED HOT-GAS ENGINE

by

KOK ANN YU

B.S.M.E., Massachusetts Institute of Technology
(1973)

SUBMITTED IN PARTIAL FULFILLMENT
OF THE REQUIREMENTS OF THE
DEGREE OF

MASTER OF SCIENCE IN
MECHANICAL ENGINEERING

at the

MASSACHUSETTS INSTITUTE OF TECHNOLOGY

May 1975

Signature of Author_____
Department of Mechanical Engineering

Certified by_____
Thesis Supervisor

Accepted by_____
Chairman, Department Committee of Graduate Students

DEVELOPMENT OF THE VALVED HOT-GAS ENGINE

by

KOK ANN YU

Submitted to the Department of Mechanical Engineering on May 5, 1975 in partial fulfillment of the requirements for the degree of Master of Science in Mechanical Engineering

ABSTRACT

This thesis is a continuation of work done on the Valved Hot-Gas Engine at M.I.T. There are two parts to this thesis - the first part measures the gas leakage past the piston rings in an attempt to determine the cause of inefficiency of the engine. The conclusion of the experiment was that gas leakage alone does not account for engine inefficiency. Heat transfer effects are believed to play an equally important role.

The second part of this thesis was the construction of a compact 60 KW electrical heater which will allow the engine to be operated closer to the maximum operating conditions.

Thesis Supervisor: Joseph L. Smith, Jr.
Title: Professor of Mechanical Engineering

AKNOWLEDGMENTS

I would like to thank Prof. J.L. Smith, Jr. for his guidance, Ron Satz who worked with me on the experiments, Karl Benner and Bob Gertsen the technicians who advised me and helped to build the heater.

I am also thankful for the research assistantship which was sponsored by the Department of Transportation (Contract No. DOT-OS-40086).

TABLE OF CONTENTS

LIST OF FIGURES

GLOSSARY OF SYMBOLS

A heat transfer area; ft^2

A_c equivalent flow area; ft^2

A_{fr} frontal area of heater core; ft^2

C_p specific heat at constant pressure; Btu/lbm°F

D inner diameter of quartz tube; ft

d_n diameter of NiCr wire; ft

d_Q diameter of quartz rod; rod ft

D_h hydraulic diameter; ft

f friction factor; dimensionless

G mass flow rate; lbm/ft^2 hr

g_c gravitational constant; 32 lbm ft/lbf sec^2

h heat transfer coefficient; Btu/ft^2 hr°F

I current; amps

L total length of NiCr wire required; ft

l length of one NiCr coil; ft

$\dot{m}$ mass flow rate; lbm/hr

P heater pressure; psi

P_c compressor pressure

P_e expander pressure

P_H pressure in high pressure line

P_L pressure in low pressure line

Pr Prandtl number; dimensionless

ρ porosity of matrix; dimensionless

$\dot{q}$ heat transfer rate; $Btu/hr\ ft^2$

R resistance; ohms

Re Reynolds number; dimensionless

r resistivity; ohm ft

r_h hydraulic radius; ft

St Stanton number; dimensionless

s length of heater core; ft

T_g gas temperature

T_n temperature of NiCr wire; °F

V voltage; volt

v specific volume of gas; ft^3/lbm

v_m $(v_1 + v_2)/2$

Subscripts

1 refers to heater inlet conditions

2 refers to heater outlet conditions

CHAPTER I

INTRODUCTION

This thesis consists of 2 parts. In the first part dynamic leakage tests were performed on the HGVE to see if it could be proved that engine efficiency was caused by piston ring leakage. The second part consists of building an electrical heater to replace the existing underpowered heater.

Tests carried out by Fryer, Hankard and Stein on the HGVE indicated an efficiency of 12.7%. This was very low compared to expected efficiency of 41.3%. To obtain the rated pressure ratio of 2, the auxiliary clearance volume for the compressor had to be set at the minimum volume. Indicated compressor power was 1.8 times the expected value. The main problem was thought to be leakage past the piston rings. From experimental data leakage from compressor to expander was calculated to be 23.6 lbm/hr and leakage from expander to compressor was 18.7 lbm/hr when averaged over the entire cycle. These figures were derived from temperature measurements and from the PV diagrams obtained on the oscilloscope.

Static tests conducted by Fryer indicated leakage from the compressor to expander to be 4.25 lbm/hr and from the expander to compressor to be 2.25 lbm/hr. These leakage rates were derived from gas bottle readings. The engine test showed a high leakage rate while the static tests showed a much lower leakage rate. This implied that leakage was dynamic.

Since gas leaks past the piston rings in both directions during operation, any direct measurement of gas leakage under operating conditions would probably indicate only net leakage past the rings. Therefore, holding the expander at a pressure always higher or lower than the compressor pressure would give an indication of the leakage in one direction. It was easier to

obtain a PV diagram than design an experiment to measure leakage directly so experiment I was designed in which P_e was held constant first at P_L and then at P_H. From the PV diagrams obtained it was not possible to identify a large leakage. In fact heat transfer seemed to play a bigger role in the PV diagrams.

In experiment II, leakage was measured directly when the expander pressure was constant and $P_L < P_e < P_H$ and when P_e was always greater than compressor pressure. Leakage in both cases was small compared to 23.6 lbm/hr. In this experiment the pressure across the piston rings did not change sign.

In experiment 3, leakage was measured when the pressure across the piston rings changed sign. Calculations based on the results of this experiment showed that leakage was one third the amount implied by Brent Fryer's measurements. These experiments failed to prove that leakage was the sole cause of inefficiency.

The second part of this thesis consisted of building a 60 KW crossed-rod electrical heater. The original heater was underpowered because it was difficult to design a 60 KW heater and because a transformer rated at 15.5 KW was available in the lab. The HGVE was designed for maximum operating conditions of 2,000 RPM, 1000 lb/in^2 expander inlet pressure, 1500°F expander inlet temperature and a 2:1 pressure ratio. The heater was of a crossed-rod matrix form, with alternate grids of fused quartz and nichrome wire. It was designed to operate on a 3 phase a.c. input.

CHAPTER II

TESTS FOR LEAKAGE ACROSS PISTON RINGS

2.1 Experiment I

The expander pressure is held constant at either P_H or P_L while the compressor is operated normally. The resulting PV diagrams are examined.

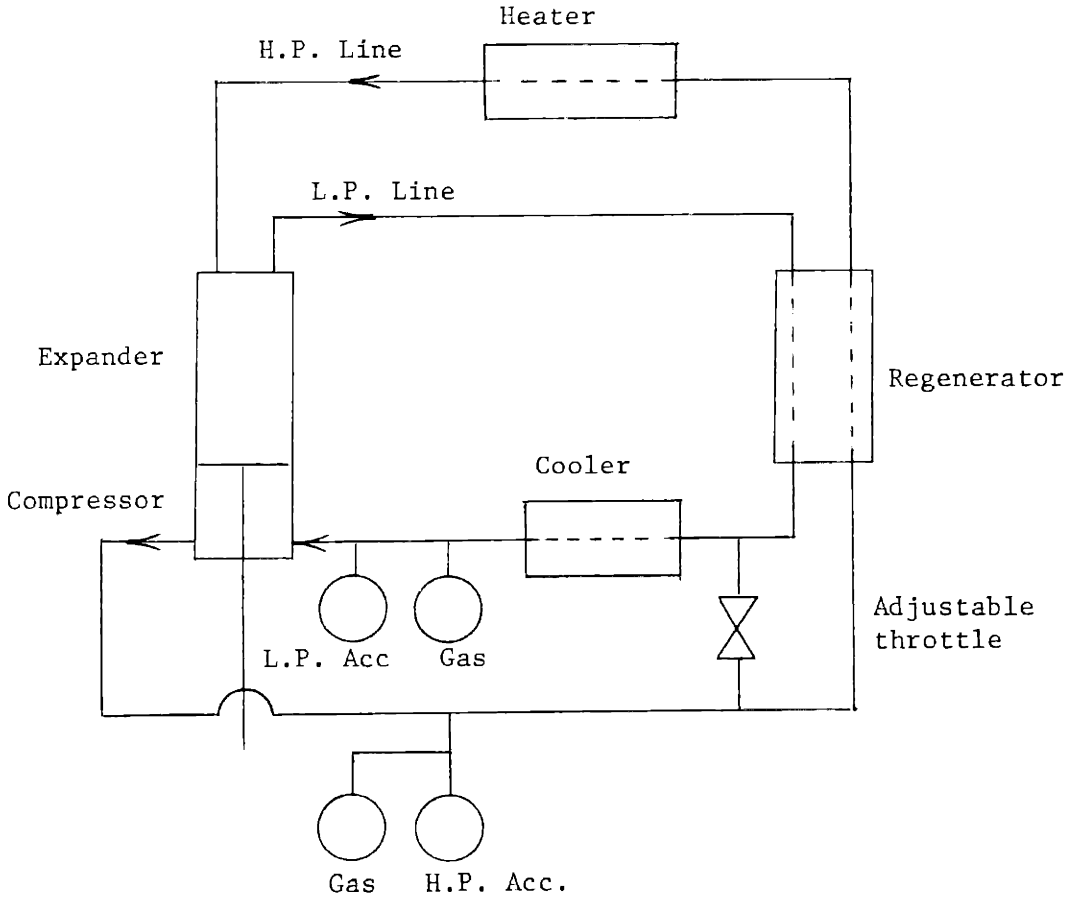

Figure 1. Engine Test Configuration for Experiment 1

The experiment

These tests were conducted at low pressures. The 0-1000 psig pressure transducers were replaced by the 0-250 psia transducers. An adjustable throttle was put in between the H.P. and L.P. lines. The gear belt was disconnected so that the camshaft was stationary. The engine was motored at just over 200 RPM. The throttle was adjusted until the pressure ratio was about 2:1. PV diagrams were photographed from the oscilloscope. More gas was let into the engine and the experiment was repeated at slightly higher pressures.

Test 1: Keep P_e constant and always lower than P_c.

Expander outlet - open; inlet - closed.

Test 2: Keep P_e constant and always higher than P_c.

Expander outlet - closed; inlet - open.

Sources of error

The main source of error was the drift in oscilloscope output. The beam was zeroed on the lowest line on the scope before each test. After taking the photo, the zero was checked and found to be ±0.2 cm off on the scope. To counteract this the engine was stopped after each photo and the pressure in the compressor was checked with a digital voltmeter. The corresponding position of the beam on the scope was noted and this served as a reference voltage for our calculations. This method is not any more accurate as the could have drifted between the time the photo was taken and the time the reference voltage was taken. The error is ±0.1in on the graphs plotted.

Results and calculations

The PV diagrams were translated very carefully from the photos to graph paper. Pressures and volumes were calculated knowing the input voltage to the

transducers and the scale on the scope. Figures 2a and 2b show the results of Test 1 and figures 3a and 3b show the result of Test 2. The ideal adiabatic expansion and compression lines are drawn for comparison.

Observations

Figures 2a and 2b do not differ significantly from figures 3a and 3b. If there were significant leakage, the compression strokes of 3a and 3b would be higher than the ideal adiabatic case. Also the expansion stroke of 2a and 2b would be lower than the adiabatic case. However, this was not the case.

The phenomena can perhaps be explained by heat transfer in the compressor. If compressor wall temperature was between T_H and T_L of the compressed gas, on the compression stroke, heat would be taken out of the gas causing pressure to be reduced and on the expansion stroke heat would be given back to the gas causing the pressure to rise.

For this experiment, heat transfer effects overshadow the leakage effects. However, the pressure difference across the piston seal did not change sign.

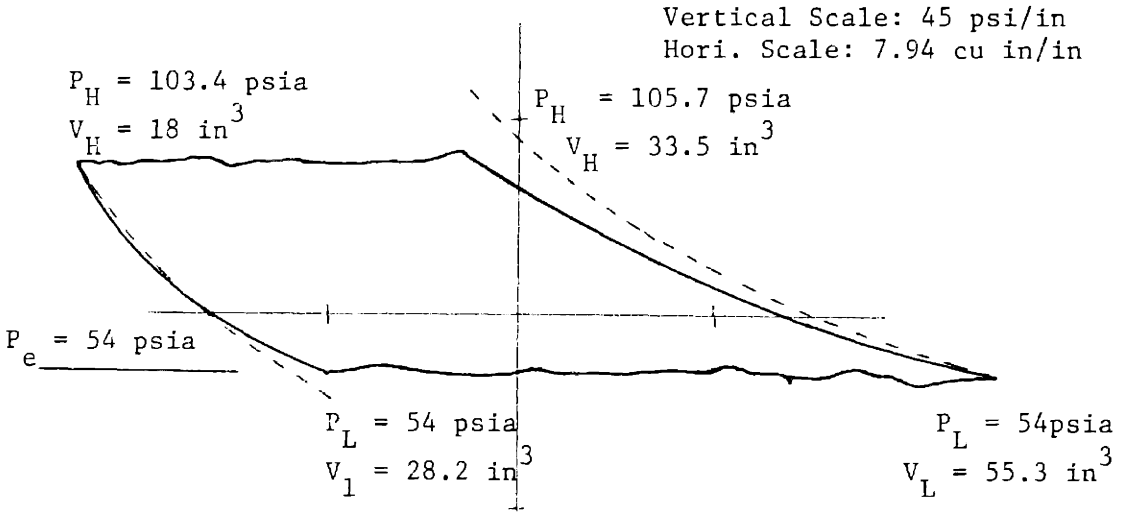

(a)

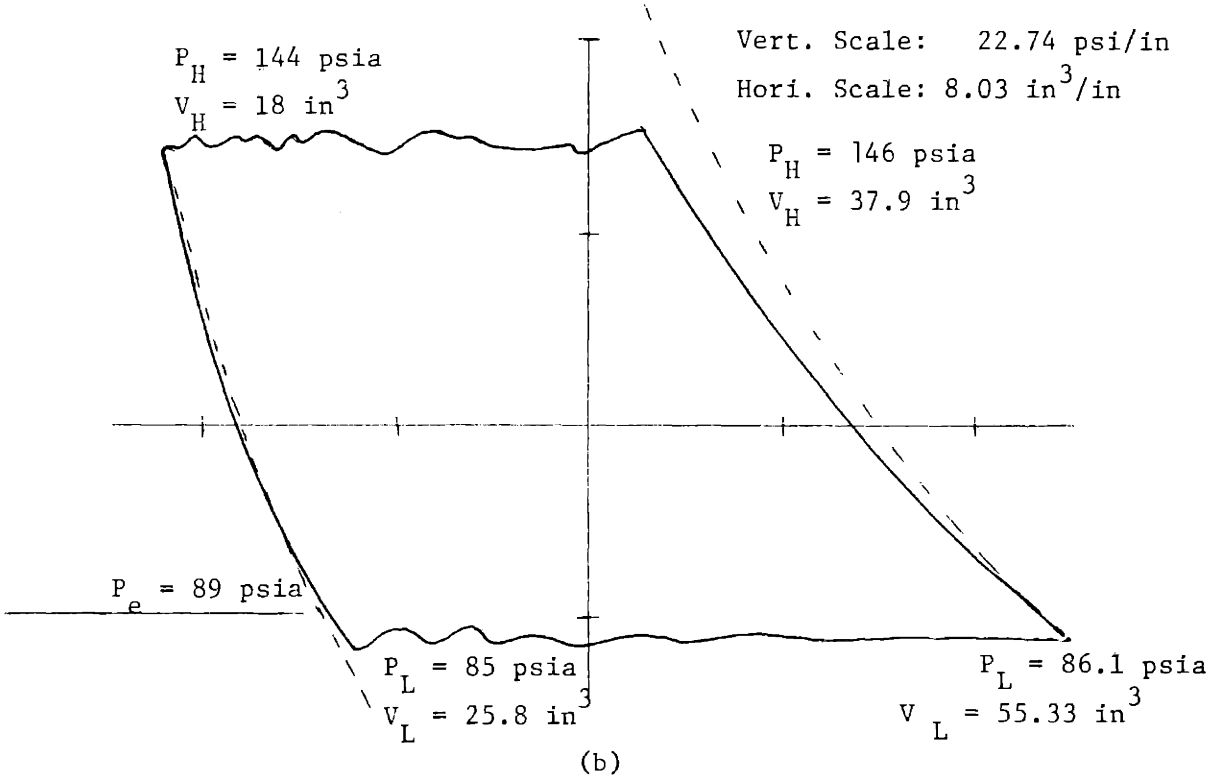

(b)

Figure 2. P-V diagrams with low expander pressure
Experiment 1, Test 1

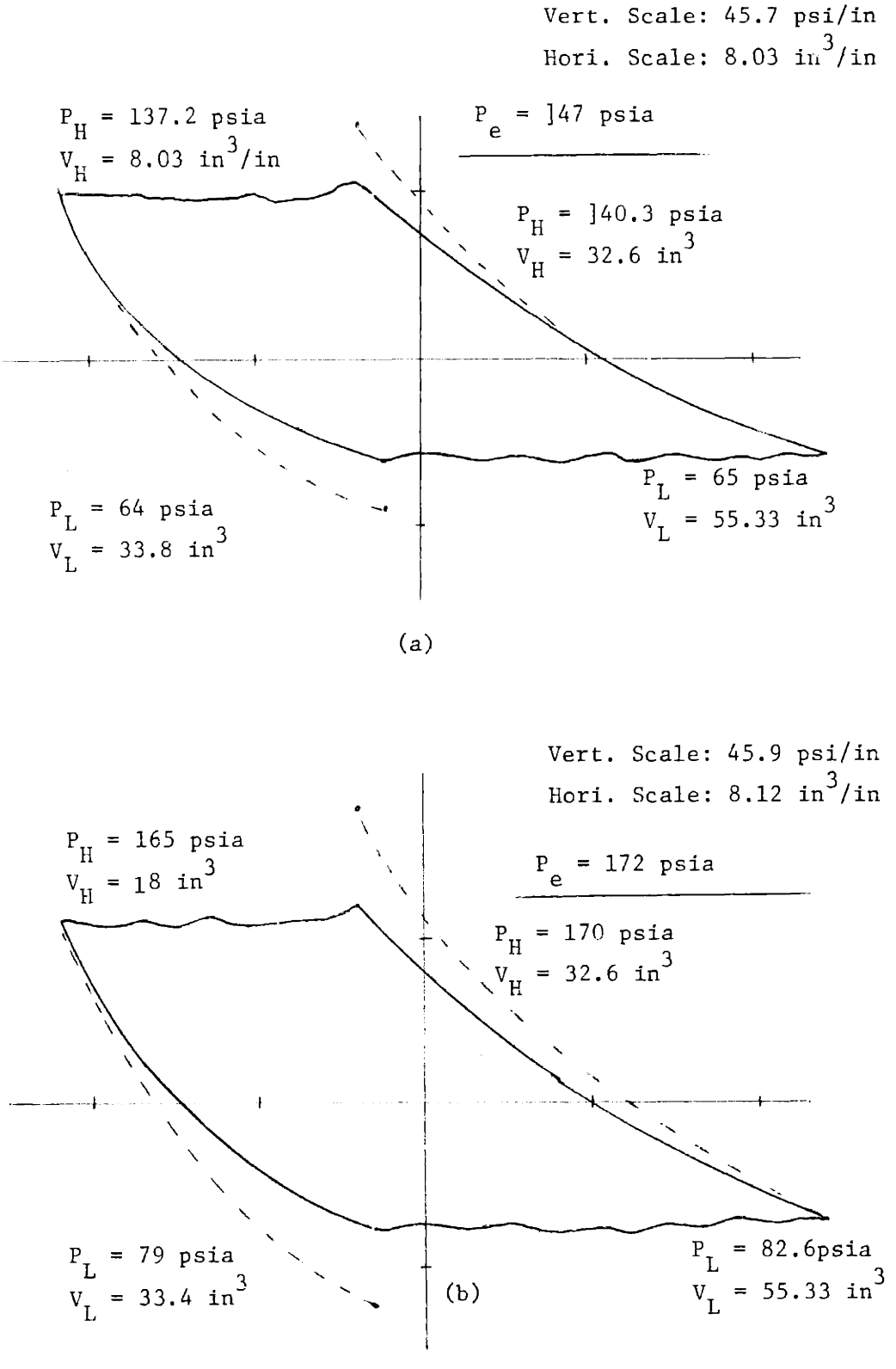

Figure 3. P-V diagram with high expander pressure
Experiment 1, Test 2

2.2 Experiment II

In this experiment, the leakage past the piston seals was directly measured. In test 3, P_e is almost constant and is at equilibrium with the compressor -- $P_L < P_e < P_H$. In test 4, P_e is almost constant and always higher than P_H in the compressor.

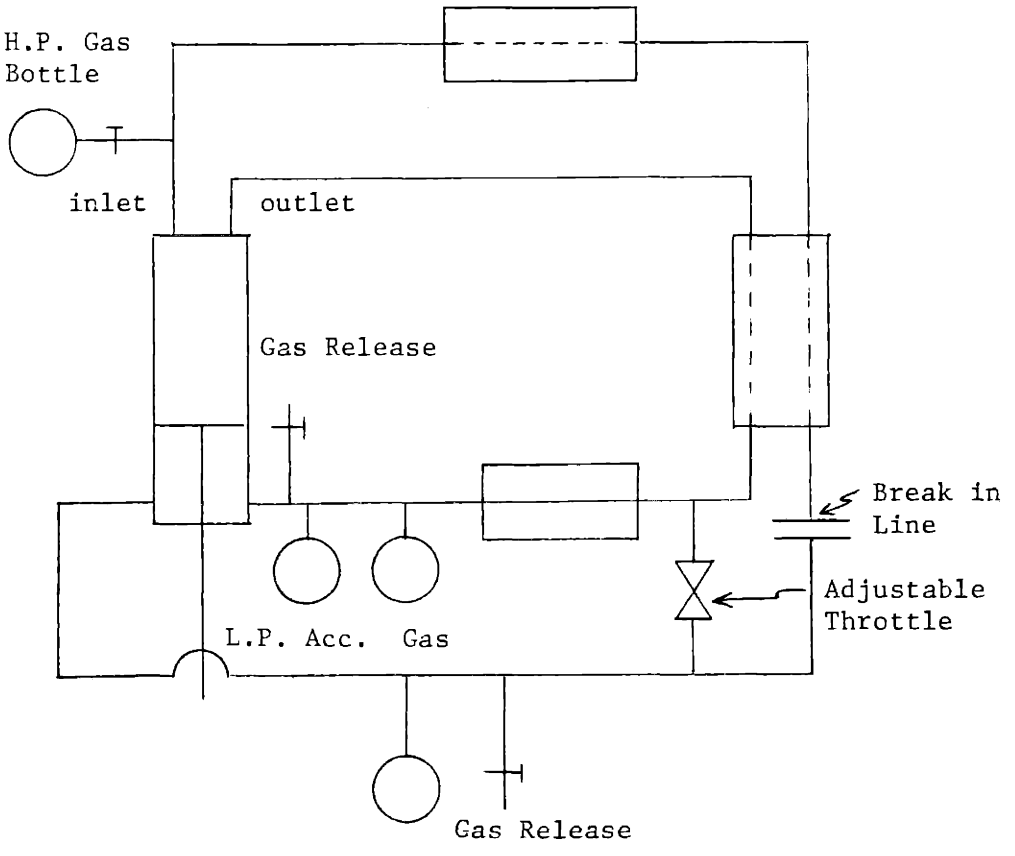

Figure 4. Engine Test Configuration for Experiment 2

The experiment

A 0 - 1000 psig pressure transducer was fitted to the expander and a 0 - 250 psia pressure transducer was fitted to the compressor. The compressor outlet was disconnected from the expander inlet by disconnecting a flanged joint and inserting a disk in between. A connection was made from a gas bottle to the inlet of the expander by means of a 1/4" copper line and a pressure gage outlet. Expander outlet valve was closed and inlet valve open. In both tests the engine was motored at 200 - 250 RPM.

Test 3

The gas supply bottles were shut. The throttle was adjusted until the pressure ratio in the compressor was 2:1. The expander cylinder was connected to the dead volume of the heater and regenerator and expander pressure was nearly constant and at equilibrium with the compressor pressure. P_e was between P_L and P_H of the compressor. Leakage occurred back and forth across the piston rings. The PV diagram of the compressor and expander were kept at their initial conditions by comparing the picture taken at the beginning of the experiment with the current picture on the scope. Gas was let into the engine from the L.P. bottle whenever engine pressure dropped. This test gave us an indication of dynamic leakage through the rod seal. The test was timed and readings of the L.P. bottle was taken at the beginning and at the end of the test.

Test 4

The L.P. gas bottle was shut and the high pressure bottle opened. The pressures were adjusted so that the pressure levels in the compressor were at the same pressures as in test 3. Pressure in the expander was regulated

and was always higher than pressure in the compressor. Gas leaked past the piston rings and caused pressure build-up in the compressor. This pressure was relieved by letting gas out to the atmosphere through a gas release valve (fig. 4). The experiment was timed and the pressure in the H.P. gas bottle was noted at the beginning and at the end of the experiment.

Results and calculations

The first test indicated that gas leaked past the rod seal at a rate of 0.22 lbm/hr when the average pressure difference between the compressor and the atmosphere was about 130 psia. The average pressure difference is defined as

$$\frac{(P_H + P_L)_{comp}}{2} - P_{atm}$$

The fourth test shows that gas leaks from the expander to the compressor at a rate of 4.5 lbm/hr when the average pressure difference between the expander and compressor was about 170 psia. The average pressure difference is defined as

$$P_{exp} - \frac{(P_H + P_L)_{comp}}{2}$$

Observations

The average pressure difference in this experiment is of the same order as in Fryer's experiment (where P_e = 535 psia, P_L = 250 psia). This experiment, however, shows a much smaller leakage than in Fryer's experiment. However, the results are not directly comparable because the pressure difference did not change sign in this experiment.

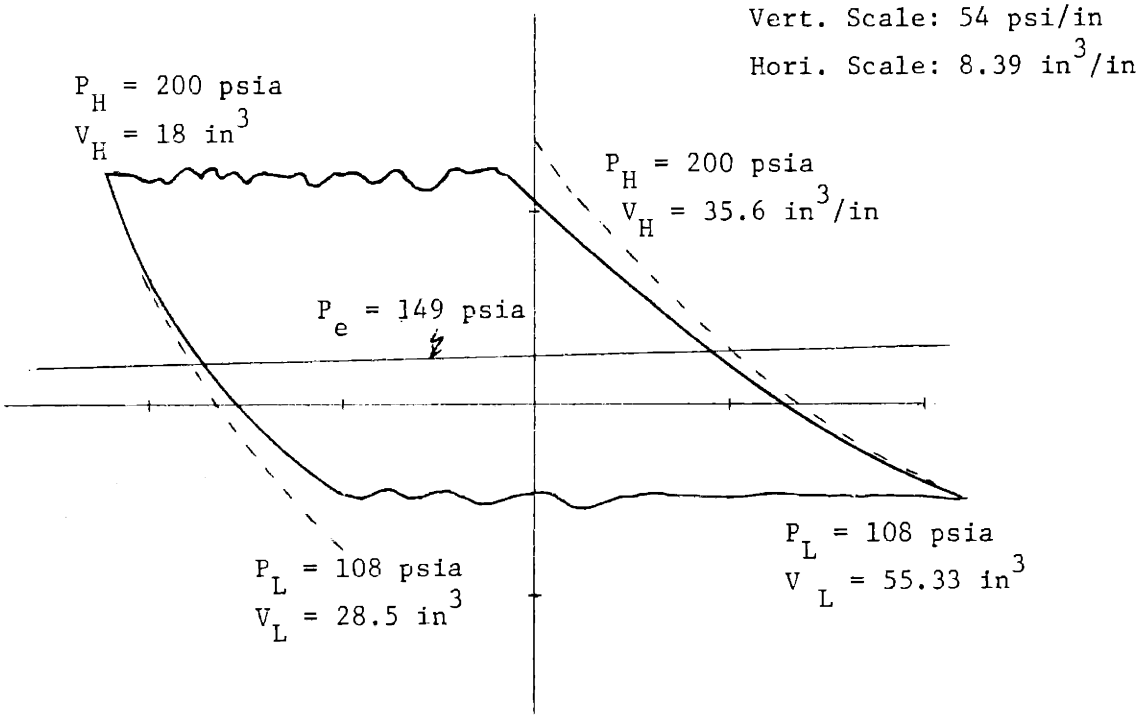

Figure 5 a. P-V diagram when expander is at equilibrium with compressor
Experiment 2, Test 3

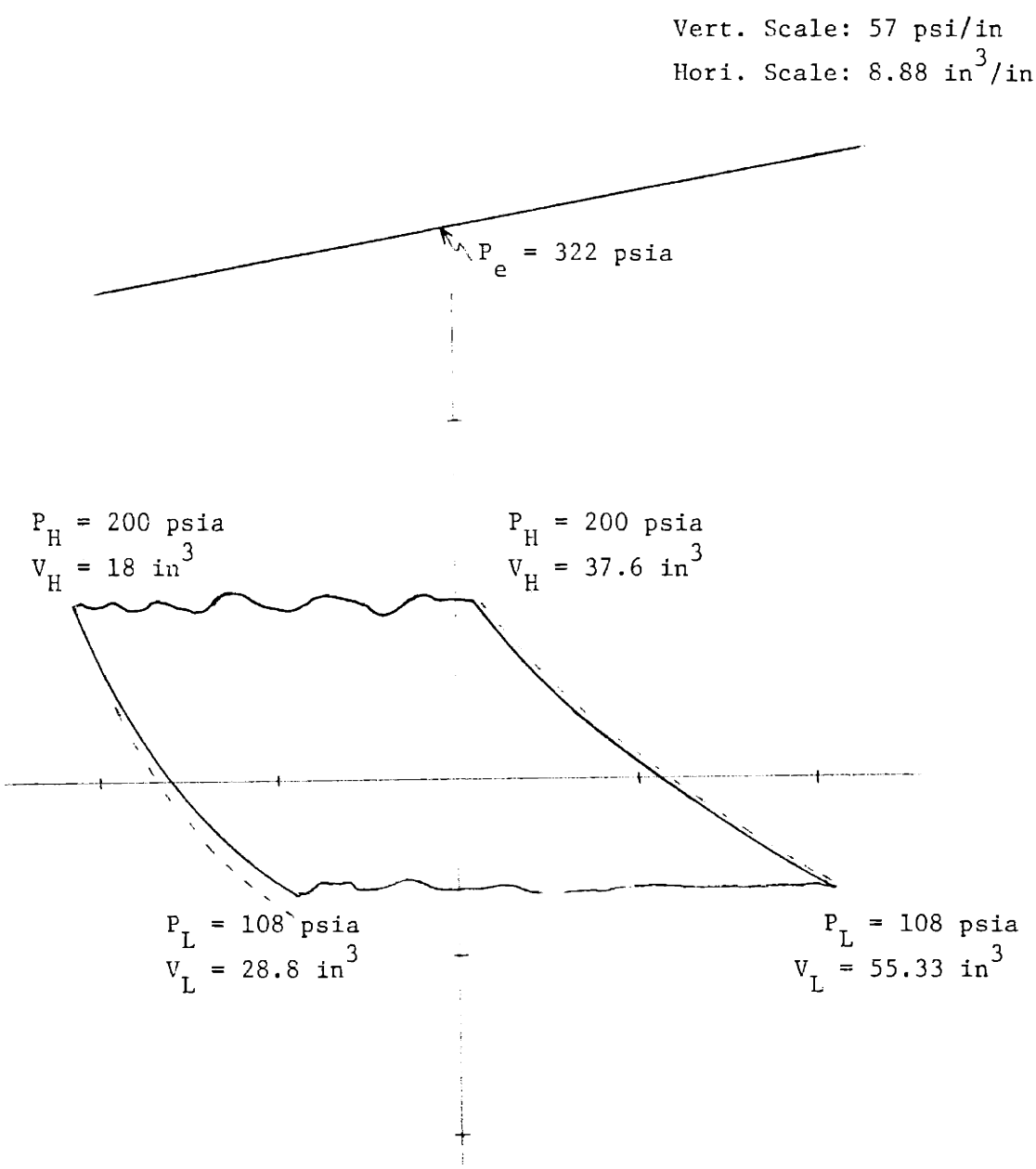

Figure 5 b. P-V diagram when expander pressure is always higher than compressor pressure

Experiment 2, Test 4

2.3 Experiment III

In this experiment we try to determine the rate of mass leakage past the piston rings when the pressure difference across the piston ring changes sign (fig. 6).

The experiment

The piston was held in position by clamping down the flywheel. This was done instead of reconnecting the flanged joint in the H.P. line. The adjustable throttle was closed. The pressure transducer outlets of the expander cylinder and compressor cylinder were modified so that they could be used for letting gas into and out of the cylinder.

The idea of the experiment was to first let $P_e > P_c$, then suddenly let gas into the compressor so that $P_c > P_e$. The rate of gas leakage could then be calculated from the pressures recorded on the oscilloscope pictures and the known volume of the expander if assumptions were made about the temperature in the cylinder.

The expander valves had to be closed, the inlet valve being held closed by pressure from the high pressure line. Ball valve 1 was initially set so that gas flowing into the expander through valve 3 leaked past the piston rings and escaped through the compressor pressure transducer outlet, finally reaching the atmosphere through ball valve 2 (see figure 6). Then valve 3 was quickly shut and immediately afterwards ball valve 2 was switched so that gas from accumulator 1 now surged into the compressor such that $P_c > P_e$. Accumulator 1 was precharged so that the pressure in it was higher than the initial pressure in the expander but lower than the pressure in the high pressure line.

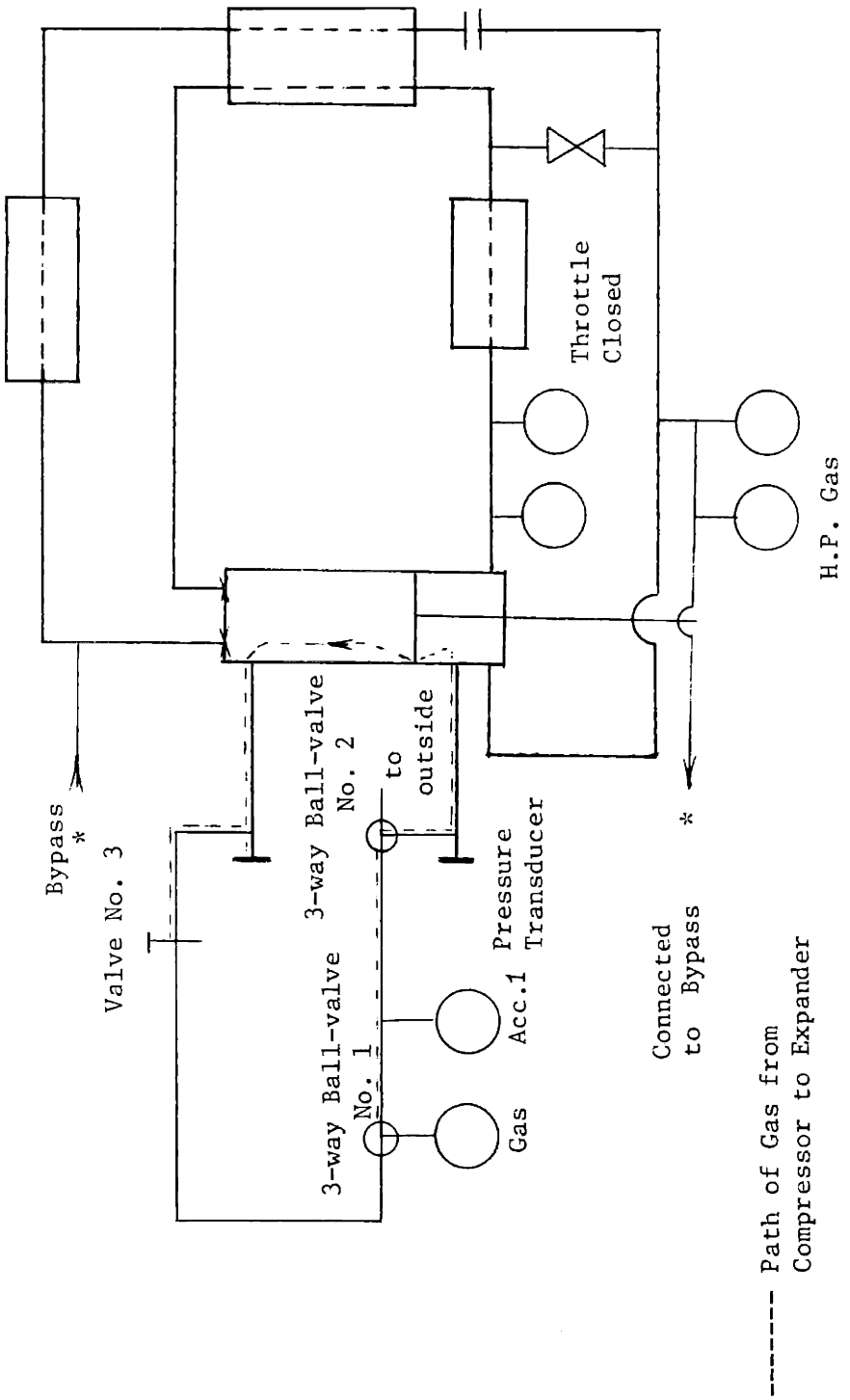

Figure 6. Direct Measurement of Leakage Past Piston Rings. Experiment 3

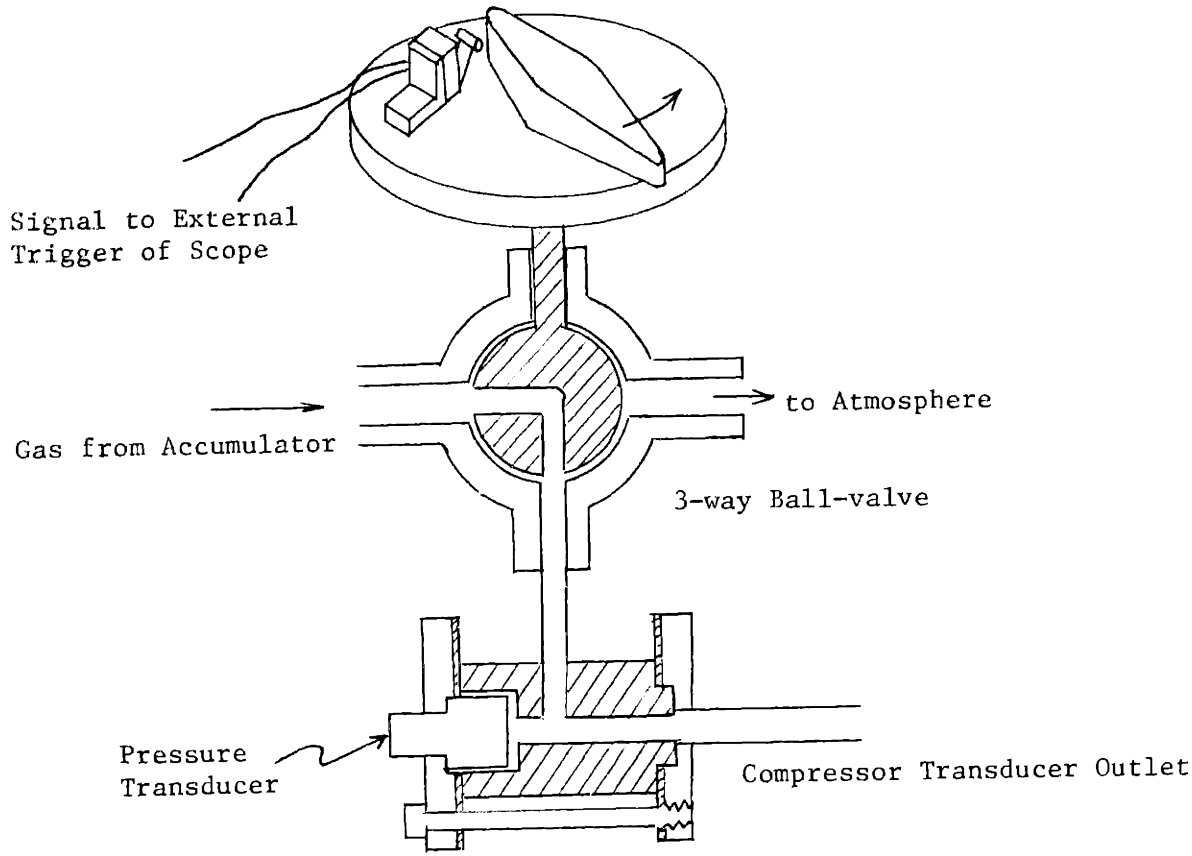

Figure 7. Mechanism to Trigger Scope Just Before Pressure Difference Changes Sign

The P vs time diagrams of the expander and compressor were recorded. There was a problem in triggering the scope with a signal from the compressor pressure transducer because the pressure fluctuations caused by gas escaping to the atmosphere prematurely triggered the scope. The problem was solved by putting a switch on ball valve 2 so that as ball valve 2 was turned to allow gas into the compressor, the switch was triggered (see fig. 7) allowing a signal to trigger the scope. The P vs t behavior of the gas in the expander and compressor were recorded on polaroid film.

Results and calculations

From the photographs, three distinctive types of pressure vs time curves can be identified. Two examples of each type are shown (figures 8, 9, and 10).

1) The leakage rate changes continuously (figures 8a and 8b).
2) One abrupt change in leakage rate after ΔP changes sign (figures 9a and 9b).
3) Two abrupt changes in leakage rate after ΔP changes sign (figures 10a and 10b).

The graphs were carefully translated from the polaroid film on to graph paper. The mass in the expander at any time can be calculated by knowing the expander volume (40.8 cu in - calculated from crank angle of 150°), the pressure (from photograph) and by assuming a temperature (room temperature). The mass in the expander can be plotted against time and the slope of the curve gives the leakage rate. The leakage rate into the expander was plotted against $\Delta P = P_c - P_e$ for the three types of cases mentioned above (see figures 11, 12, and 13: curve a in figure 11 corresponds to data from figure 8a; curve b in figure 11 corresponds to data from figure 8b, etc.).

Observations

Figure 8 shows the piston rings may not have sealed properly on the upper part of the groove. The abrupt change in leakage in figure 9 shows the rings may have sealed properly all at once and figure 10 may indicate that partial sealing occurred when some rings sealed and more complete sealing occured when all the rings sealed.

Comparing figures 11, 12, and 13, the following observations can be made:

1) When ΔP reaches 60 psi (figs. 12 and 13), the leakage rate changes abruptly.
2) In case 1 (fig. 11), ΔP did not exceed 60 psi.
3) In case 3,(fig. 13), there was a second abrupt change at ΔP = 120 psia.

Estimate of leakage during actual running of engine

It is assumed that piston ring leakage during the actual running of the engine behaves like the leakage behavior shown in figure 12, i.e., there is one equation describing leakage for ΔP from 0 to 60 psi and another equation describing leakage for ΔP greater than 60 psi. It is also assumed that leakage from expander to compressor behaves in the same way as leakage from compressor to expander. The empirical equations are fitted thru the data of figure 12 (see figure 14).

For $\Delta P < 60$ psi: $\dot{m}_e = K_1 \Delta P^2$ $K_1 = 2.17 \times 10^{-7}$

For $\Delta P > 60$ psi: $\dot{m}_e = K_2 \Delta P^{1/2}$ $K_2 = 2.35 \times 10^{-4}$

where the subscript e stands for experimental and $\dot{m}_e$ is measured in lbm/s and ΔP is measured in psi.

As a first approximation, assume that leakage resembles incompressible flow, i.e. leakage is proportional to $\frac{P_m}{T_m}$

$$\frac{1}{P_m} = \frac{1}{2}\left(\frac{1}{P_e} + \frac{1}{P_c}\right)$$

Since the temperature at the cold end of the piston is about the same during the experiment and during actual running, we neglect temperature effects.

During the actual running of the engine:

$\Delta P < 60$ psi: $\dot{m}_a = K_1 \Delta P^2 \frac{P_m}{P_{ref}}$ $P_{ref} = 90$ psi

$\Delta P > 60$ psi: $\dot{m}_a = K_2 \Delta P^{1/2} \frac{P_m}{P_{ref}}$ $P_{ref} = 140$ psi

Subscript a stands for actual. P_{ref} is the average mean pressure during the experiment used to determine K_1 and K_2. P_m and ΔP are calculated for every 3 degrees of crank angle for the actual running of the engine.

Figure 15 shows calculated leakage during actual running. The absolute value of leakage is plotted. (Leakage is always from the high pressure to the low pressure side.) Gas leakage calculations are summarized in Table 1.

TABLE I

Calculated Gas Leakages

Compressor to Expander		Expander to Compressor	
$\Delta P < 60$ psi	1.07	$\Delta P < 60$ psi	0.52
$\Delta P > 60$ psi	7.06	$\Delta P > 60$ psi	4.79
TOTAL	8.13 lbm/hr	TOTAL	5.31 lbm/hr

As is shown by Table 1, most of the gas leaks when the pressure difference is greater than 60 psi, i.e., when the piston rings are not in transition. Gas leakage is about 1/3 that implied by Brent Fryer's measurements.

(a)

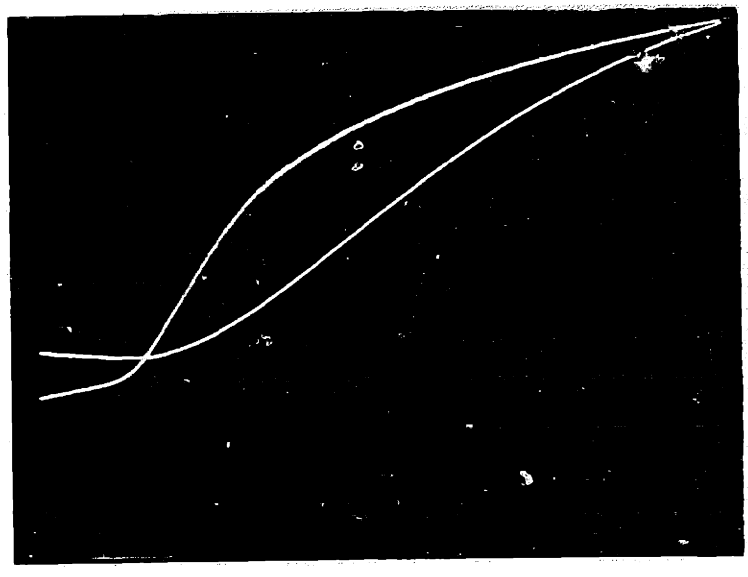

(b)

Figure 8. Pressure vs Time Pictures from Oscilloscope - No Abrupt Changes in Leakage Rate. (Vertical Scale: 1 division = 27 psia Horizontal Scale: 1 division = 50 ms)

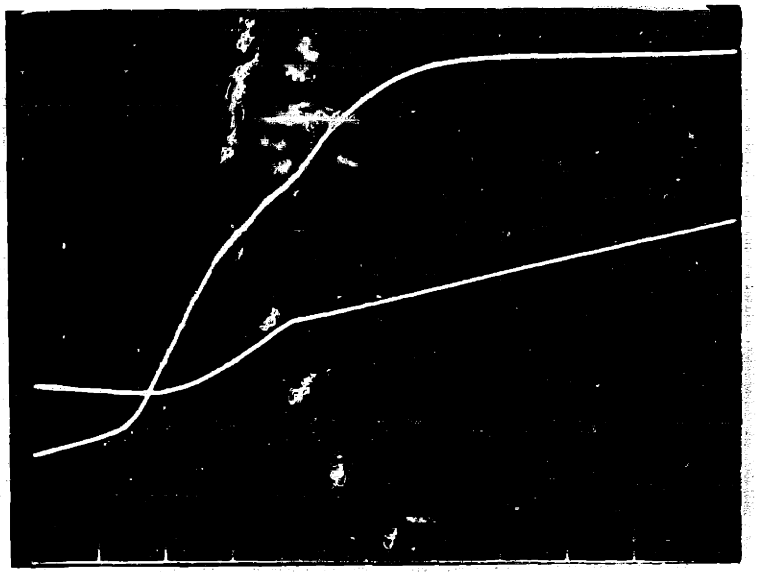

(a)

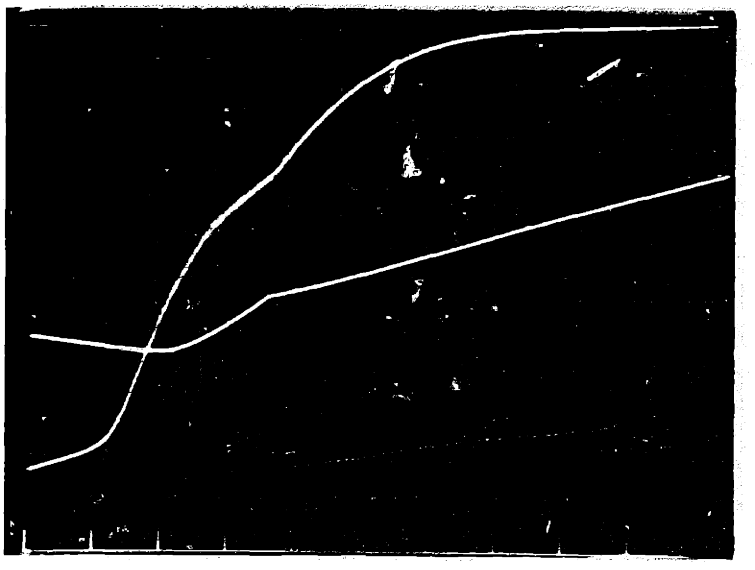

(b)

Figure 9. Pressure vs Time Pictures from Oscilloscope - One Abrupt Change in Leakage Rate. (Vertical Scale: 1 division = 27 psia Horizontal Scale: 1 division = 50 ms)

(a)

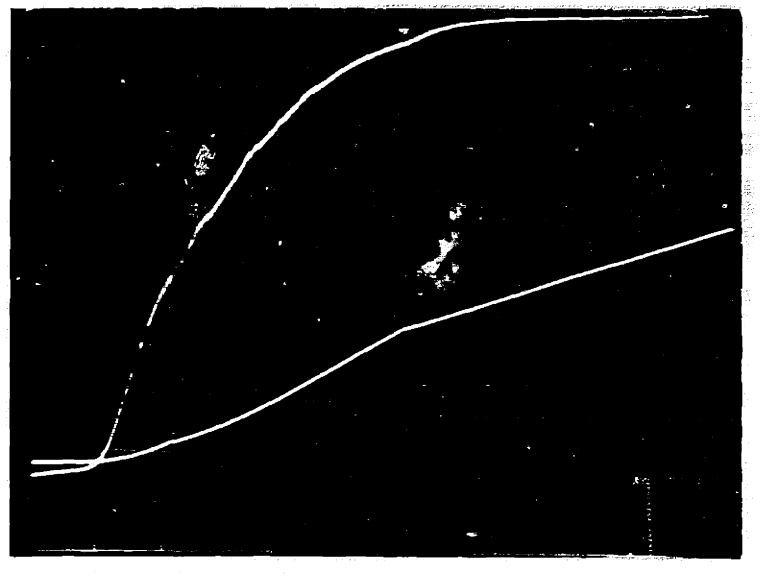

(b)

Figure 10. Pressure vs Time Pictures from Oscilloscope - Two Abrupt Changes in Leakage Rate. (Vertical Scale: 1 division = 27 psia Horizontal Scale: 1 division = 50 ms)

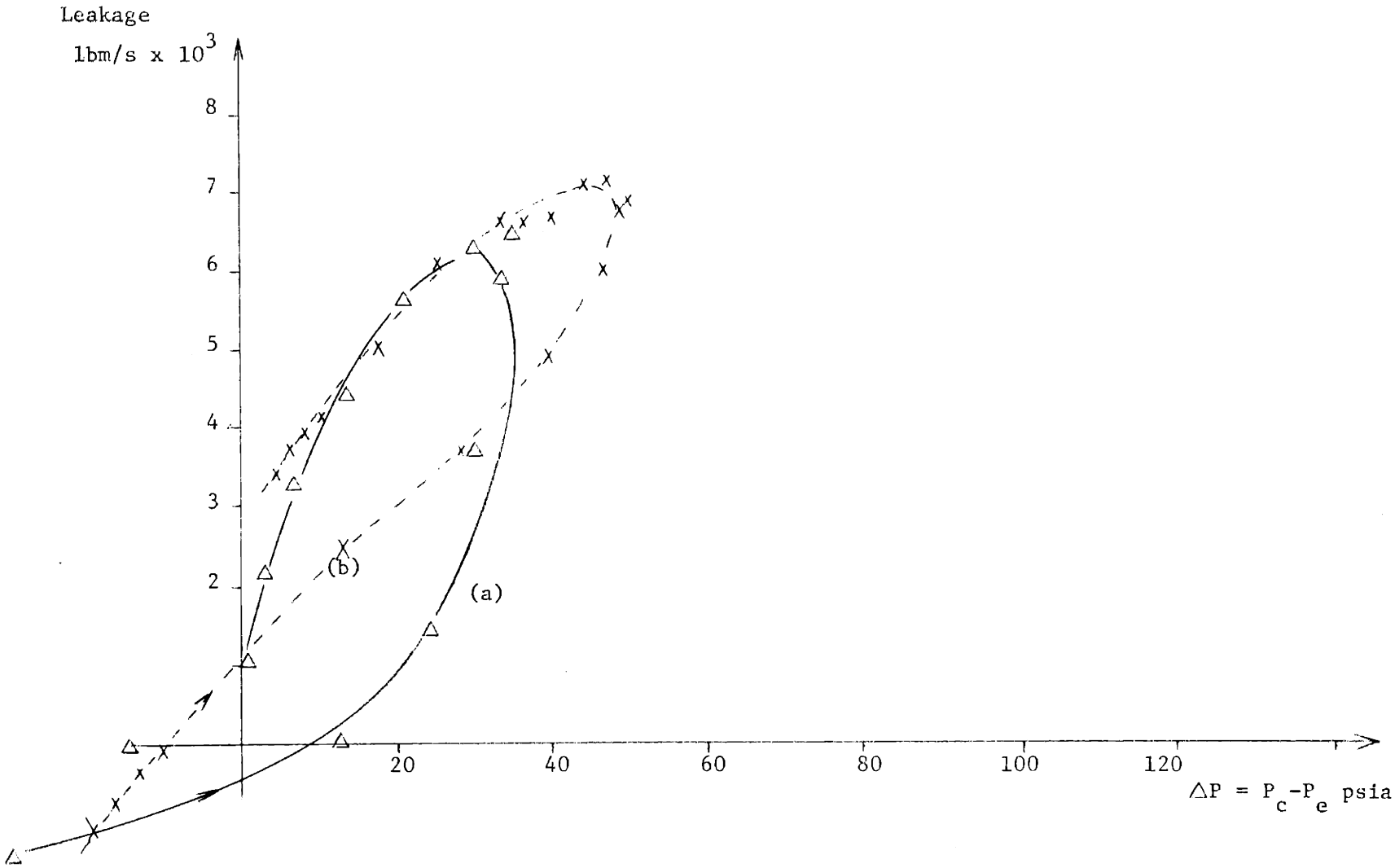

Figure 11. Leakage Past Piston Rings vs Pressure Difference - No Abrupt Change in Leakage Rate. (Data from Figures 8a and 8b)

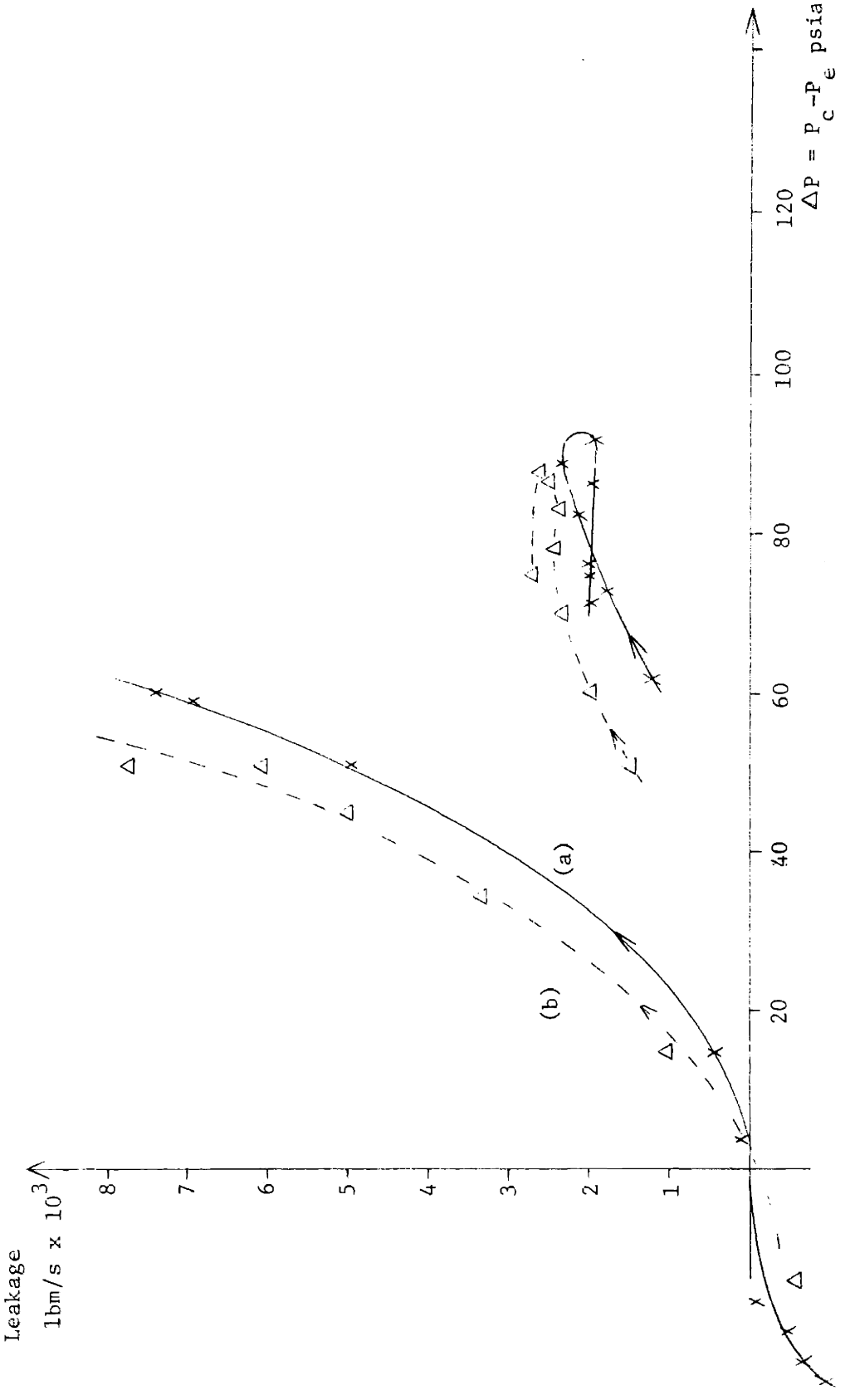

Figure 12. Leakage Past Piston Rings vs Pressure Difference - One Abrupt Change in Leakage Rate. (Data from Figures 9a and 9b)

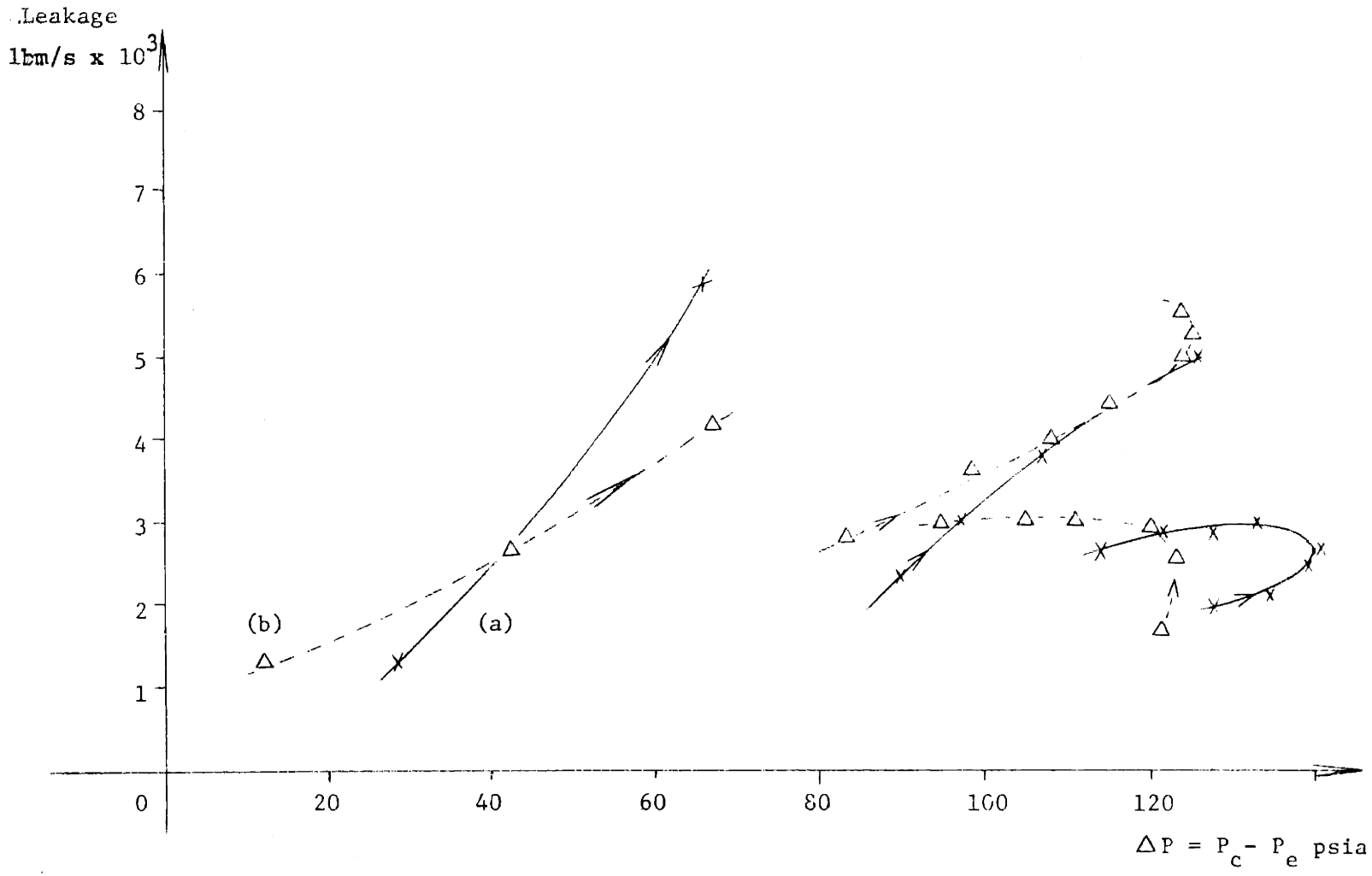

Figure 13. Leakage Past Piston Rings vs Pressure Difference - Two Abrupt Changes in Leakage Rate. (Data from Figures 10a and 10b)

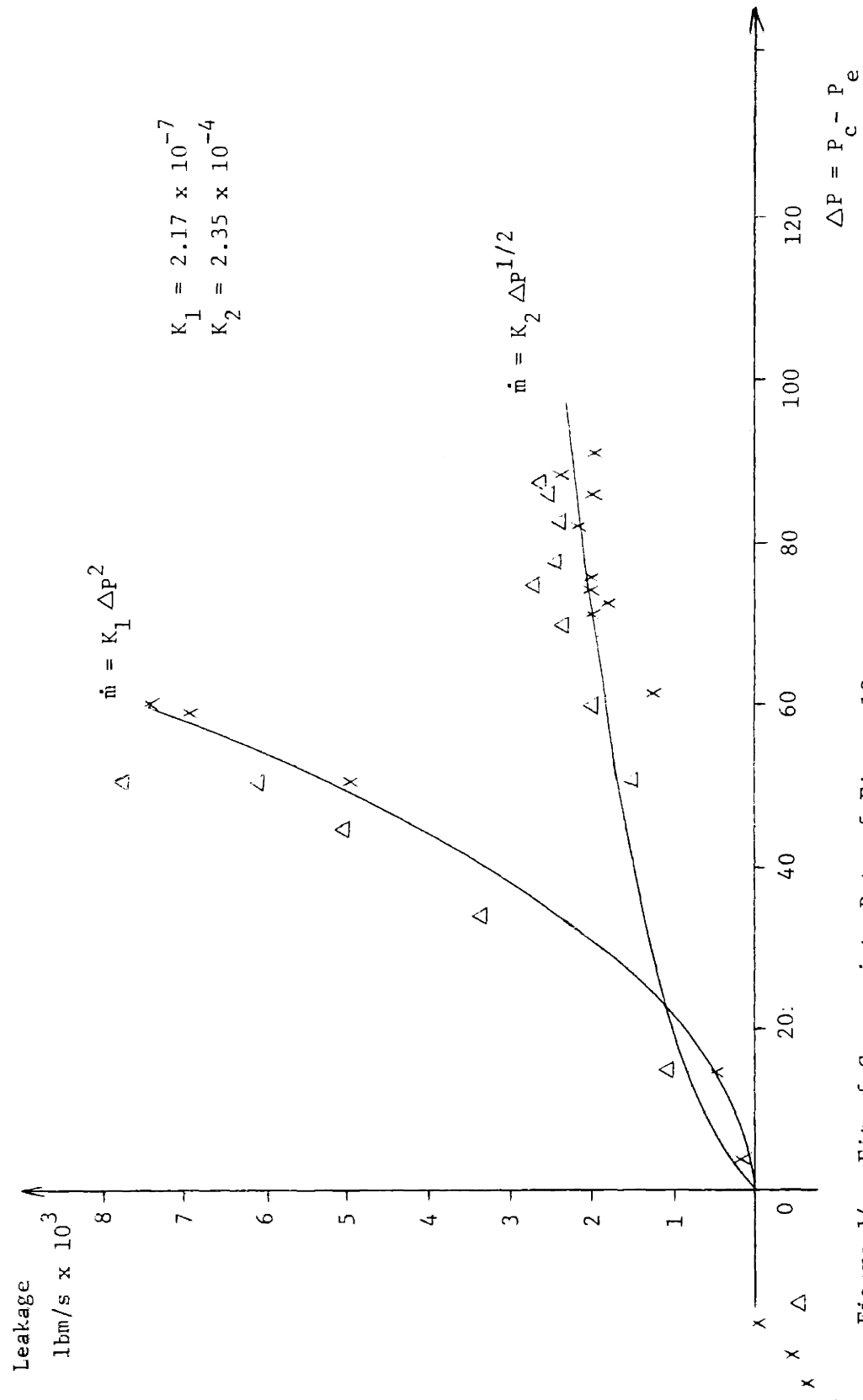

Figure 14. Fit of Curves into Data of Figure 12

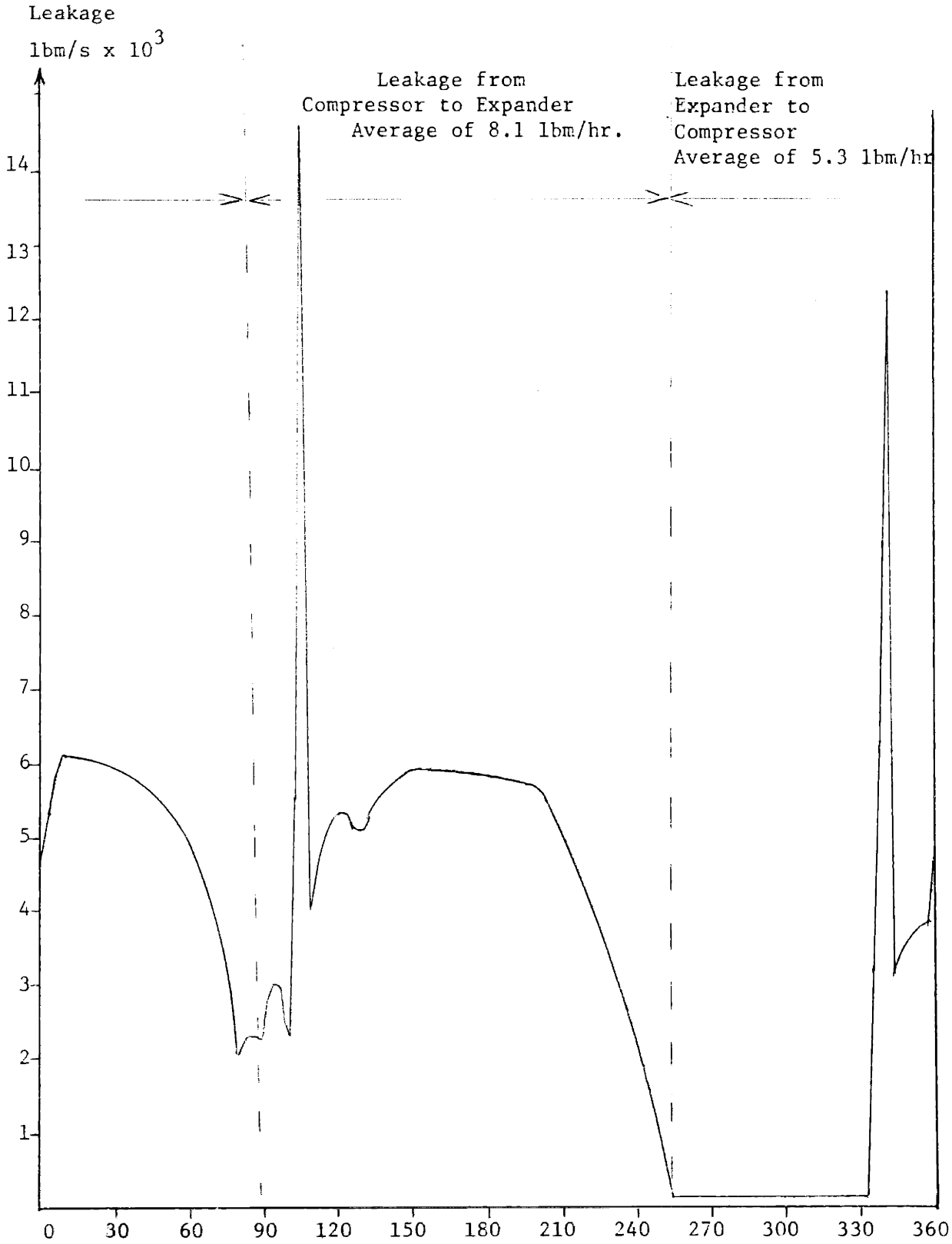

Figure 15. Mass Leakage from High Pressure Side into Low Pressure Side of Cylinder vs Crank Angle.

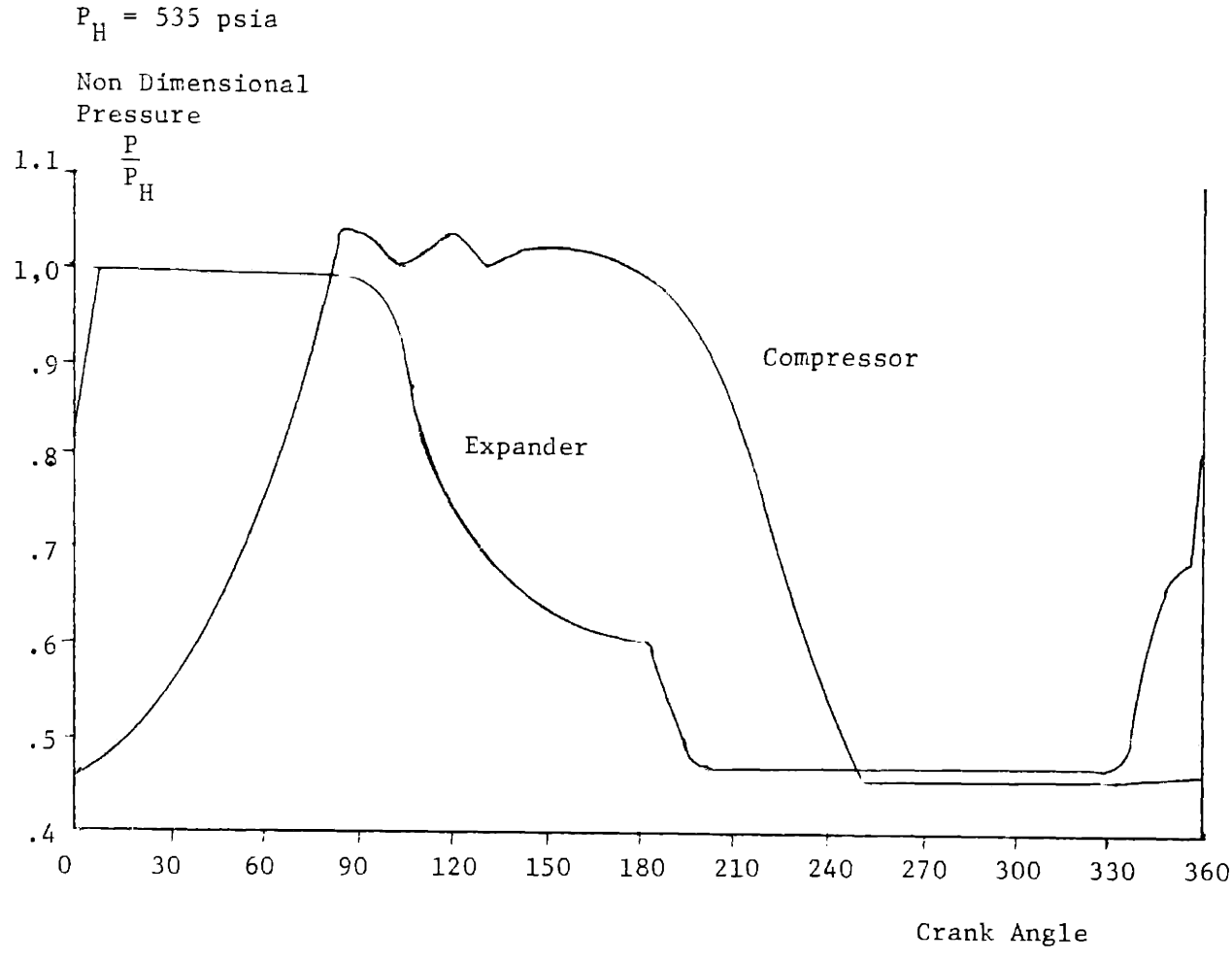

Figure 16. Pressure vs Crank Angle for the Expander and Compressor (Experimental)

CHAPTER III

DESIGN AND CONSTRUCTION OF THE HEATER

3.1 Description of the Heater

The heater is comprised of two basic components: the heater core and the high pressure heater shell. The materials used to build the heater are listed in Appendix 4.

Heater Core

The heater core is of a crossed rod matrix design. Flat serpentine grids of gage 10 nichrome wire are alternated with flat quartz serpentine grids (fig. 17, Appendix 1). The nichrome grids are connected end to end by welds using nickel filler rod. The quartz grids were bent up from 3 mm quartz rods. There are a total of 90 NiCr grids. The grids are placed inside a 64 mm O.D., 60 I.D., 21 inches long quartz tube. (There were excessive gaps between the Nichrome and quartz matrix and the quartz tube. These gaps were filled with quartz tubes so that gas would flow through the matrix instead of around it.) The ends of the quartz tube and the heater matrix are axially supported by stainless steel end plates which are perforated with holes to allow gas to flow through. A radial hole was made near the hot end of the tube to allow a thermocouple for measurement of matrix temperature to pass through. The thermocouple is insulated with an alumina sheath. This sheath is not attached to the Nichrome wire.

Three phase A.C. power enters the heater core by means of 3 nickel rods which connect to the corners of the delta connected heater. A delta connection was made because it minimizes voltage levels at the phase boundaries in the heater. The nickel leads are insulated with 3 mm I.D., 5 mm O.D. quartz tubes. The peak voltage difference across any two leads is 295 volts.

Heater Shell

The heater shell is sized for a 1000 hr rupture stress of 1000 psi and at 1500°F. The electrical leads and the thermocouple are passed through the heater shell in 3 electrical glands at the cold end and a thermocouple gland at the hot end of the heater. Teflon packings in the glands prevent gas from escaping to the environment and water jackets cool the outer ends of the glands to prevent the teflon from being overheated. The leads are connected to the heater by loops of nickel wire. These loops provide flexibility to take up the relative motion when the heater core expands at a different rate from the heater shell. The nickel lead rods are sized to allow minimum heat leakage through the leads (Appendix 2).

3.2 Heat Transfer Characteristics

At maximum operating conditions gas enters the heater at 982°F and leaves at 1500°F. The gas temperature will increase linearly with distance down the heater since the heater power is uniform. Maximum output of the heater is 210,000 But/hr. The heater wire temperature will also increase linearly with distance. The temperature difference between the wire and the gas is calculated to be at most 239°F.

REFERENCES

1) Shoichi Furuhama and Masaru Hiruma, "Axial Movement of Piston Rings in the Groove". Presented at the 27th ASLE Annual Meeting in Houston, Texas, May 1 - 4, 1972.

2) Shoichi Furuhama and Hiroshi Ichikawa, "L-Ring Effect on Air-Cooled Two-Stroke Gasoline Engines". SAE Abstract 730188.

3) Aue, G.K., "On the Mechanism of a Piston Ring Seal", Sulzer Technical Review, Jan. 1974. Published by Sulzer Brothers, Limited, CH-8401, Winterthur, Switzerland.

4) Fryer, Brent C., "Design, Construction and Testing of a New, Valved Hot-Gas Engine", Doctoral thesis, M.E., MIT, February 1972.

5) Hankard, Thomas K., "Instrumentation and Testing of a Closed, Reciprocating, Brayton Cycle Engine", Engineers thesis, M.E., MIT, May 1973.

6) Stein, Robert, "A Progress Report on the Development of the Valved, Hot-Gas Engine", Masters thesis, M.E., MIT, January 1974.

7) Macosko, Block, Lumannick and Richter, "A Compact 90 KW Electrical Heat Source for Heating Inert Gases to 1700°F", NASA Technical Memorandum X-52778, March 1970.

8) Rohsenow, Warren M. and Choi, Harry, "Heat, Mass, and Momentum Transfer", 1961 by Prentice Hall, Inc.

9) Kays, William and London, A.L., "Compact Heat Exchangers", McGraw-Hill Series in Mechanical Engineering.

10) Den Hartog, J.P., "Strength of Materials", 1949, McGraw-Hill Book Company, Inc.

Appendix 1. Heater Core Design and Structure

Individual Grids

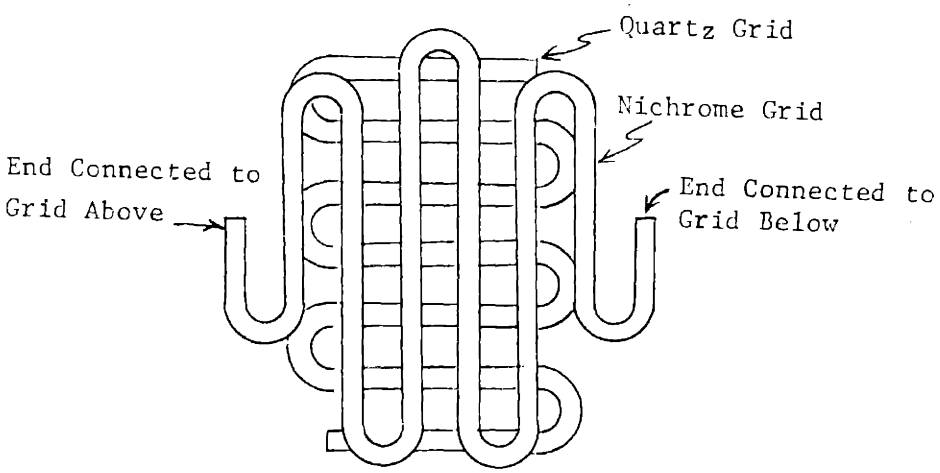

Figure 17. Alternating Grids of NiCr and Quartz (Actual Size)

Heater Core Structure

The NiCr grids are connected in the manner shown in Figure 18. Because of space limitations in the core, the Ni rods were connected to the coils in a way such that resistance was distributed with a nonuniformity of $\pm$ 3.3 percent. The next section shows that the temperature distribution in the core was not significantly changed because of this nonuniformity.

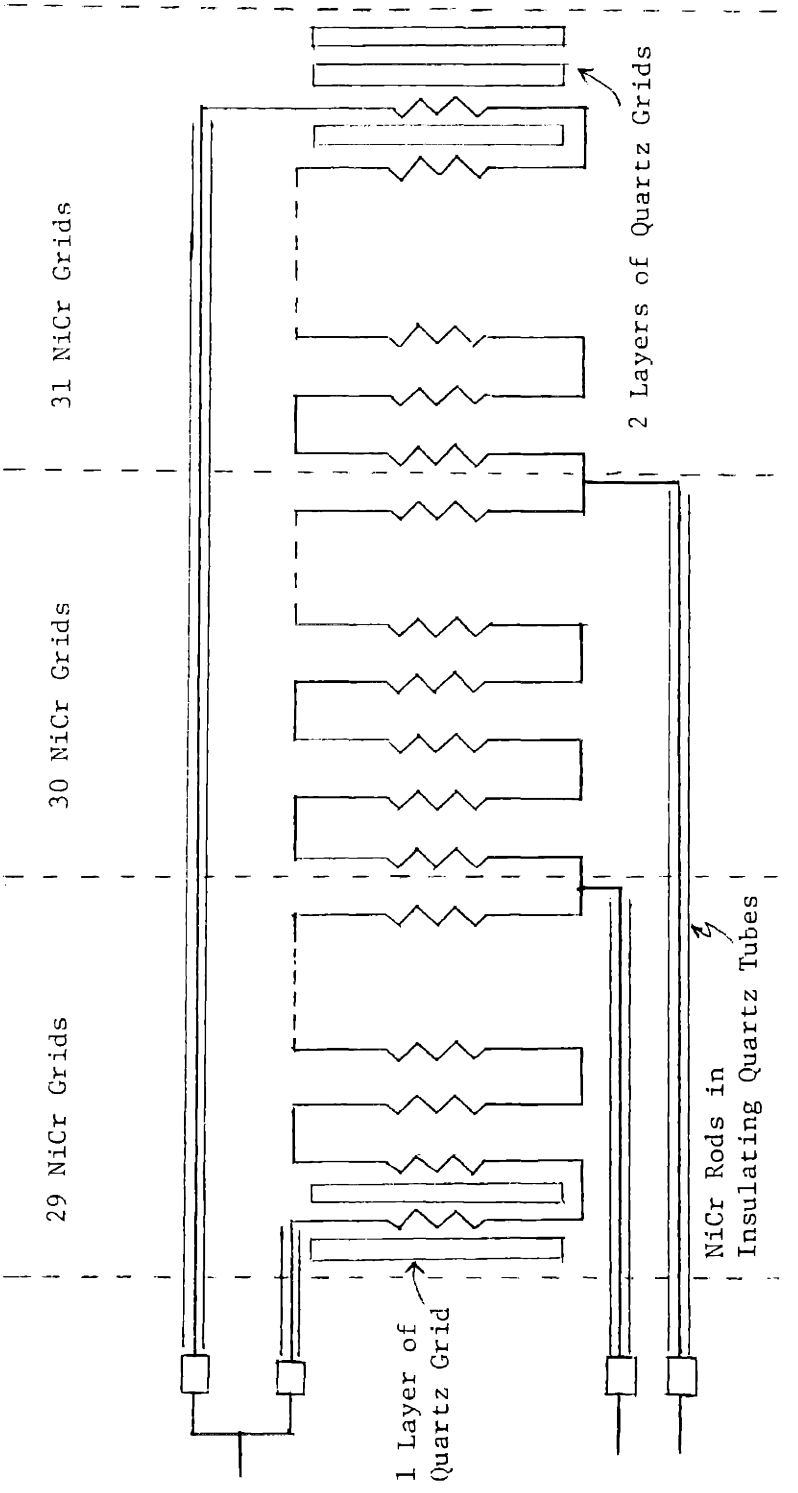

Figure 18. Schematic Arrangement of NiCr and Quartz Grids in Heater.

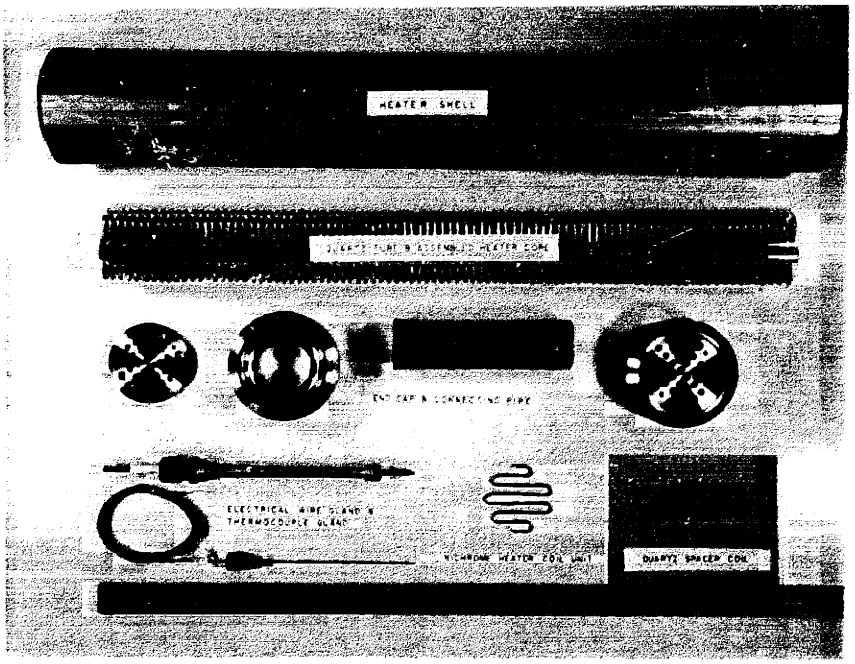

Heater Assembly

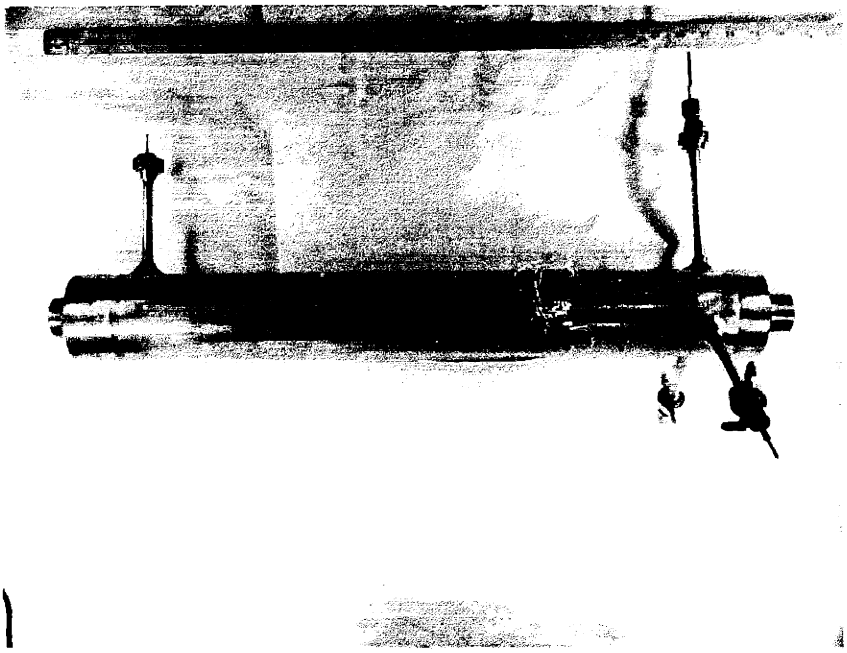

Assembled Heater

Figure 19.

Heater Wire Temperature Distribution

Power generated in each phase of core

$$\dot{Q} \propto \frac{V^2}{R}$$

$$\propto \frac{1}{R} \text{ when V is constant}$$

For each phase, $(T_{out} - T_{in})$ gas $= \frac{\dot{Q}}{\dot{m}C_p} \propto \frac{1}{R}$ where $\dot{Q}$ is in Btu/hr

$$(T_n - T_g) = \frac{\dot{q}}{Ah} \propto \frac{1}{R} \text{ where } \dot{q} \text{ is in Btu/hr ft}^2$$

Each phase of core would have 30 resistance grids with combined resistance R if the core were uniform and the phase balanced.

$$(T_{out} - T_{in})' = (T_{out} - T_{in}) \frac{R}{R'},$$

$$(T_n - T_g)' = (T_n - T_g) \frac{R}{R'},$$

where R' is the resistance of the unbalanced phase.

The temperature of the wire and gas are calculated and the results shown in figure 20. We see that the temperatures of the NiCr and gas in the cold end are raised and at the hot end, wire temperature is lowered slightly. Final gas outlet temperature is hardly affected.

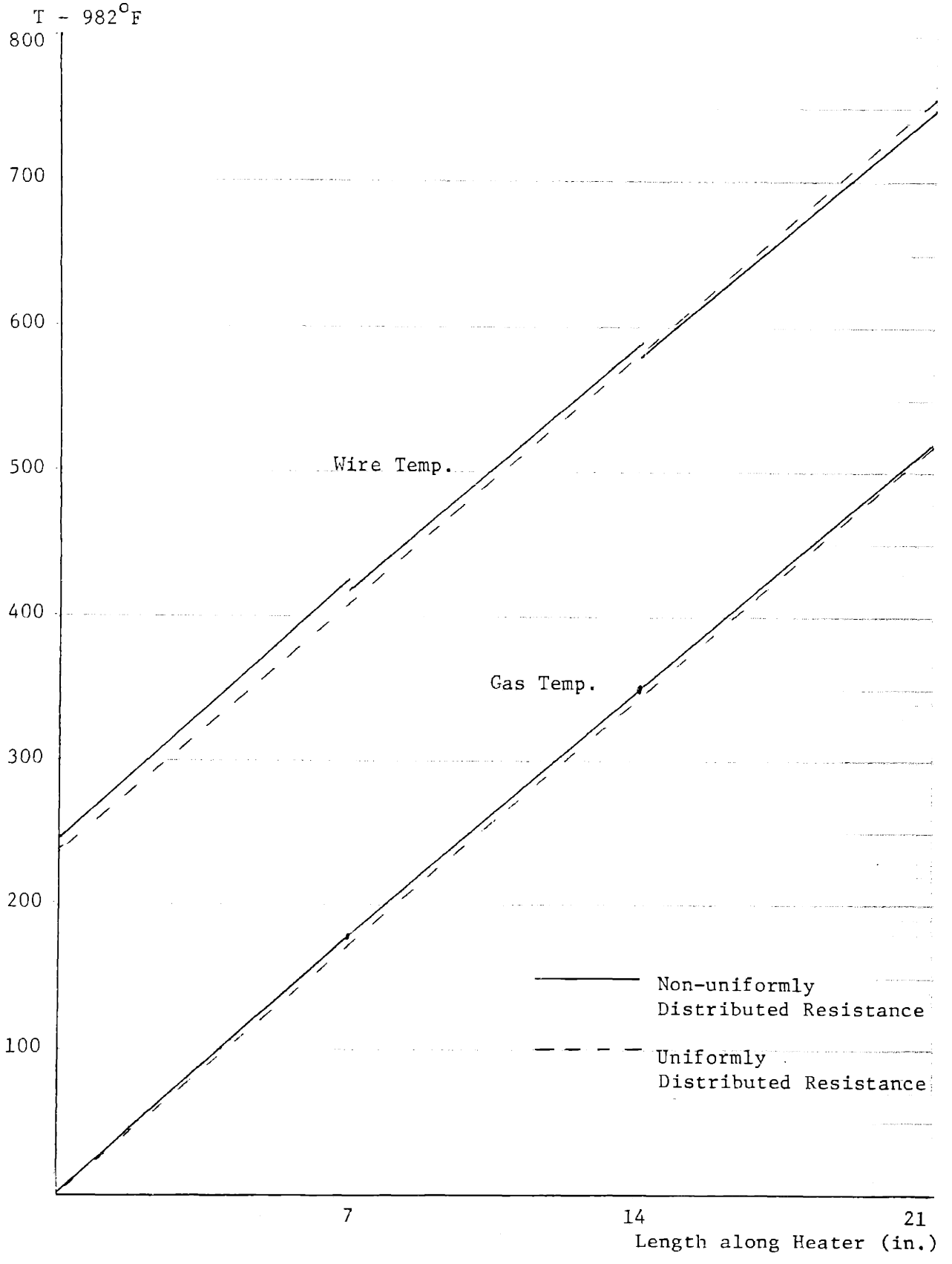

Figure 20. Wire and Gas Temperatures of a Non-uniformly Distributed 3 phase Heater

Appendix 2. Optimization of Area/Length Ratio on Ni Lead Rod

We want to minimize heat loss from the heater out through the nickel leads. Assume that the Ni lead is insulated except at the ends. Assume that the cool end of the Ní lead is at room temperature. The A/L equation is from Appendix 8 of Fryer. Minimum heat loss occurs when

$$\frac{A}{L} = \frac{I^2 r}{2(T_w - T_s)k_m}$$

where A = cross section area of lead

L = length of lead

I = current

r = resistivity

k_m = thermal conductivity

T_w = temperature of heater wall, T_s = temperature of sink.

The maximum RMS current is 169 amps,

$r = 2.765 \times 10^{-7}$ ohm ft

$k_m = 52$ Btu/ hr ft°F

$T_w = 1500°F$

$T_s = 80°F$

1 watt $\equiv$ 3.413 Btu/hr

$A/L = 4.272 \times 10^{-4}$

Suppose L = 5", the diameter of the lead should be 0.1807 inches.

Heat loss from Ni lead:

$$\dot{q} = k_m \frac{A}{L}(T_w - T_s) + \frac{I^2 r}{2}\frac{L}{A}$$

$$= 41 \text{ Btu/hr}$$

Heat loss from stainless steel sheath:

Assume heat is rejected only from the ends.

$$\dot{q} = k_s \frac{A}{L}(T_w - T_s)$$

For $D_o = 0.430$ in

$D_i = 0.257$ in

$k_s = 10$ Btu/hr ft°F

$\dot{q} = 22.1$ Btu/hr

Appendix 3. Heat Transfer and Pressure Drop Calculations for Heater Core

Gas flows only during 0.3 of each period. When gas flows it flows at a maximum rate, $\dot{m}$, of 1080 lbm/hr. The average (overtime for entire period) rate of heat transfer

$$\dot{q} = 0.3\ \dot{m}\ C_p(T_2 - T_1) \tag{1}$$

$$= 210{,}000 \text{ Btu/hr}$$

Assume that no heat transfer occurs during the 0.7 period that gas is not flowing. Therefore, the actual rate of heat transfer during 0.3 period is $\dot{q}/0.3$

$$\frac{\dot{q}}{0.3} = Ah(T_n - T_g) \tag{2}$$

Since heat flux $\dot{q}/A$ is constant along the heater, the gas increases linearly in temperature as a function of distance. h depends on R_e, P_r and core geometry and is the same everywhere since the gas properties are essentially independant of temperature. Therefore, $(T_n - T_g)$ is constant and the temperature of the Nichrome increases linearly with distance.

We can set a miximum $T_n - T_g$ so that the maximum temperature of the wire is 1500°F + $(T_n - T_g)$, and then select the matrix geometry and the flow area. Knowing G we can calculate R_e and then determine h from data given by Kays and London. The heat transfer area A can now be found from equation (2) and the length of the heater core can be determined.

Pressure drop calculations can be performed to see if they are reasonable.

Heat Transfer Calculations

We are looking for a maximum $(T_n - T_g)$ of 200°F to 300°F.

Core geometry:

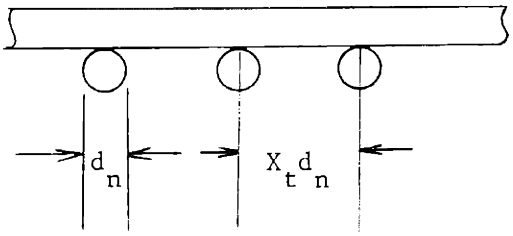

Choose X_t,

$$\rho = 1 - \pi/4\ X_t$$

$$r_h = d_n(X_t/\pi - 0.25)$$

Choose D,

$$A_{fr} = \frac{\pi D^2}{4}$$

$$A_c = \rho A_{fr} \qquad \text{by definition}$$

$$G = \frac{1080}{A_c}$$

$$R_e = \frac{GD_h}{\mu}$$

From Kays and London for a crossed rod matrix,

$\frac{h}{GC_p} P_r^{2/3}$ and f are determined from R_e and X_t

Calculate h

A can now be determined: $A = \frac{\dot{q}}{0.3h(T_n - T_g)}$

Length of NiCr wire required $L = \frac{A}{\pi d}$

$$n = \frac{L}{l}$$

$$s = n(d_n + d_Q)$$

d_n and d_Q should be the same in using the Kays and London charts but in reality they are slightly different.

Pressure Drop Equation

$$\frac{\Delta\rho}{P_1} = \frac{G^2}{2g_c}\frac{v_1}{P_1}\left\{(1 + \rho^2)\left[\frac{v_2}{v_1} - 1\right] + f\frac{s}{r_h}\frac{v_m}{v_1}\right\}$$

Electrical Requirements at Maximum Output

Max. power required	61.5 KW
Resistance of each phase	~2.15 ohm
Power in each phase	20.5 KW
RMS current in each phase	$I = \sqrt{\frac{20,500}{2.15}}$
	= 97.6 amps
Line current $=\sqrt{3}\ I$	= 169 amps

RMS voltage across any two lines V_{RMS} = 210 volts

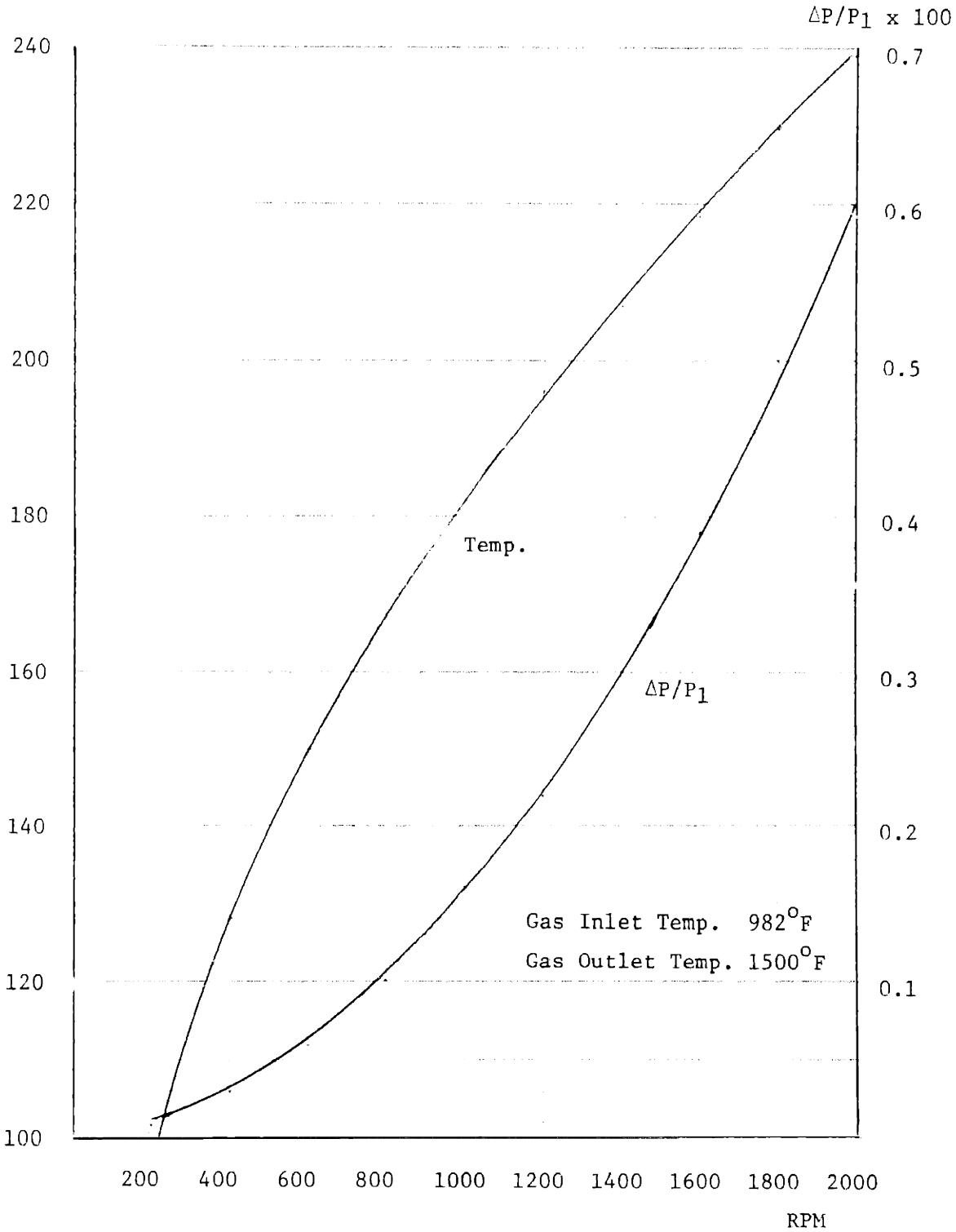

Figure 21. Heater wire Temperature and $\Delta P/P_1$ as a Function of Engine Speed.

Appendix 4.

Heater Specifications

Max. power	60.5 KW
Volts/phase (RMS)	210 volts
Current/phase (RMS)	98 amps
Line current (RMS)	169 amps

Nichrome wire

Diameter (gage 10)	0.102"
Length of each grid	13.13"
Number of grids	90
Resistance (total)	6.44 ohms
Resistance of each phase -	
29 grids	2.1 ohms
30 grids	2.15 ohms
31 grids	2.2 ohms

Quartz Rod

Diameter	3 mm
Number of grids	92

Quartz Tube

O.D.	64 mm
I.D.	60 mm
Length	21"

Nickel Leads in Heater Core

O.D.	0.110"
Quartz insulation for leads	
I.D.	3 mm

O.D.	5 mm

Electrical Feed Throughs

Ni rod - O.D.	0.187"

Jacket

316 SS Schedule 160

I.D.	2.626"
O.D.	3.5"

Connecting Pipes

O.D.	1.66"
I.D.	1.265"

Hot end: SS316

Cold end: SS304

Electrical Feedthrough Glands

Stainless steel with teflon seal.

Thermocouple Gland

Stainless steel with teflon seal.

Thermocouple

Chromel alumel

Thermocouple sheath: SS, ungrounded, O.D. 0.062" reduced to 0.040 at the tip

Basis for Calculations

Temperature of gas at inlet	982°F
Temperature of gas at outlet	1500°F
Maximum calculated wire temperature	1739°F
Maximum flow rate (during 0.3 period)	0.30 lbm/sec
Engine RPM	2000

X_t 3

Gas Properties, etc. (taken at average temperature of 1240°F)

C_p = 1.242 Btu/lbm°F

k_g = 0.176 Btu/hr ft°F

μ = 0.103 lbm/hr ft

P_r = 0.73

$R_e(max)$ = 10,470

Appendix 5. Sources of Components, Materials, and Information

Chromel A (Nichrome) Wire	Malin Co. 5400 Smith Road Brook Park, Ohio 44142 Contact Miss Stanton (216-267-8090)
Nickel Rods	Metal Goods Glenn and Ames Streets Marlborough, MA 01752 Contact Mr. Gosselin (617-899-9649)
Quartz Rod	Quartz General Corp. 9 Lake Street Wakefield, MA 01880 Contact Mr. Frank Ducharme (617-246-0550)
Conax Electrical Glands and Thermocouple Gland	Charles T. Morgan Co., Inc. 500 Maple Street Hathorne (Danvers), MA 01937 Contact Mr. Stephen Lunn